Biometals (2012) 25:351–360
DOI 10.1007/s10534-011-9506-6

Biogenic synthesis of multidimensional gold nanoparticles assisted by *Streptomyces hygroscopicus* and its electrochemical and antibacterial properties

Sathya Sadhasivam · Parthasarathi Shanmugam · Murugan Veerapandian · Ramesh Subbiah · Kyusik Yun

Received: 7 July 2011 / Accepted: 27 October 2011 / Published online: 9 November 2011

Abstract The fabrication of reliable, green chemistry processes for nanomaterial synthesis is an important aspect of nanotechnology. The biosynthesis of single-pot room-temperature reduction of aqueous chloroaurate ions by *Streptomyces hygroscopicus* cells has been reported to facilitate the development of an industrially viable greener methodology for the synthesis of technologically important gold nanoparticles (AuNPs). Multidimensional AuNPs are generated via the manipulation of key growth parameters, including solution pH and reaction time. The synthesized nanostructures are characterized by UV/Vis and energy dispersive X-ray analysis studies. Particle morphology is characterized by HRTEM, FE-SEM and BioAFM. Additionally, we have demonstrated the electrochemical and antibacterial properties of AuNPs via cyclic voltammetry analysis and a minimal inhibitory concentration assay. Owing to the drawbacks of chemical synthesis, a biological synthesis method has been developed to generate biocompatible, inexpensive and eco-friendly size-controlled nanoparticles.

S. Sadhasivam · M. Veerapandian · R. Subbiah · K. Yun (✉)
College of Bionanotechnology, Kyungwon University, Gyeonggi-Do 461-701, Republic of Korea
e-mail: ykyusik@kyungwon.ac.kr

P. Shanmugam
Department of Biotechnology, Bharathidasan University, Trichy, Tamil Nadu 620024, India

Keywords Gold nanoparticle · Nanostructure · Multidimensional · Electrochemical

Introduction

Multi-structured nanomaterials have attracted increasing attention because they are not only of fundamental interest but also potentially useful (Brus 1994; Johnson et al. 2001; Duan et al. 2003). Biological methods using bacteria and fungi for the synthesis of metal (Klaus et al. 1999; Hosea et al. 1986; Mukherjee et al. 2001; Ahmad et al. 2003; Brown et al. 2000) and semiconductor (Ahmad et al. 2002, 2003; Dameron et al. 1989; Labrenz et al. 2000) nanoparticles represent a relatively unexplored and underexploited alternative, but have hitherto yielded minimal results in terms of size and shape control. Biological systems could synthesize and assemble a range of inorganic nanomaterials such as amorphous silica (diatoms) (Kroger et al. 1999) magnetite (*Magnetotactic* bacteria) (Lovley et al. 1987) and minerals such as calcite (Herman et al. 1988) into functional superstructures. Understanding the biochemical processes that lead to the formation of nanoscale inorganic materials is therefore potentially appealing as an environmentally friendly alternative to chemical methods for nanoparticle synthesis. Living organisms have the endogenous ability to regulate the synthesis of inorganic materials. For example, shape and size control of inorganic nanomaterials in biological systems has been achieved

either by the formation of membrane vesicles (Lang et al. 2007) or through functional molecules such as polypeptides that bonded specifically to mineral surfaces (Komeili et al. 2004). Many microbial species have been found to be capable of synthesizing metal nanoparticles but without much success in achieving shape control. However, the high-yield synthesis of nanoparticles with anisotropic shapes such as nanorods, nanotriangles, hexagons and pentagons remains a challenging task for nanochemists, and frequently requires complex and time-consuming steps such as morphology transformation from the nanospheres or seeded growth processes. On the other hand, it has been discovered that many biological organisms, both unicellular and multicellular, are capable of producing inorganic nano materials, either intra or extra-cellularly, with anisotropic morphology and hierarchical assembly, frequently to nanoscale dimensions (Iosin et al. 2008).

Among the nanomaterials, coinage metals such as Au, Ag and Cu are regarded as multifunctional materials useful for a broad range of applications; gold nanoparticles (AuNPs) are of great value in this regard, owing to their unique physico-chemical and biological properties. By controlling the size and shape of AuNPs, the versatility of these techniques could be improved. Thus, the development of new methodologies for controlled synthesis of AuNPs is essential for several research applications (Wong et al. 1998; Tang et al. 2002; Grubbs 2007). From the promising results of our previous work [biosynthesis of AgNPs by *S. hygroscopicus,* (Sadhasivam et al. 2010)], we extend the present research work by biosynthesizing the AuNPs. In our study, *S. hygroscopicus* was utilized as bio-nanofactory machinery to reduce the levels of chloroauric acid and modulate the formation of multidimensional AuNPs such as spheres, triangles, and hexagons. *S. hygroscopicus* has been recognized as a very important microorganism for the production of several antibiotics and enzymes. The results obtained in the present study have further demonstrated the nanosynthesis applications of *S. hygroscopicus*. In order to elucidate the properties of biosynthesized AuNPs, several analytical techniques were conducted. For instance, maximum absorbance and crystalline properties were studied via UV–visible and X-ray diffraction spectroscopy, respectively. Elemental composition and morphological characteristics were also significantly characterized.

It is very important to address the potential applications of synthesized biocompatible nanomaterials. However, reports on their applications have proven quite limited, with the exception of antimicrobial studies. In this regard, in the current study, along with their anti-bacterial properties (against 4 gram-positive and 2 gram-negative bacteria), the electrochemical properties of biosynthesized AuNPs were evaluated. Several bio-analytical devices have been designed by incorporating the unique properties of AuNPs (Iosin et al. 2008; Katz et al. 2004). They have the ability to provide a stable surface for the immobilization of biomolecules that retain their biological activities (probably as the result of enhanced orientational freedom) is extremely useful when preparing biosensors. Nanomaterials composed of multi-dimensional ensembles of nanoparticles (NP) are becoming increasingly important in analytical and materials chemistry. Indeed, applications in nanoelectronic devices, optoelectronic devices, chemical sensors, and catalysts appear imminent (Schmid 1998; Heath et al. 1998; Bethell and Schriffrin 1996; Lee et al. 2004). Furthermore, electrochemical biosensors created by coupling biological recognition elements with electrochemical transducers based on or modified with AuNPs have played an increasingly important role in biosensor research over the past few years. In this report, cyclic voltammetry was utilized to study the fundamental electrochemical properties of biosynthesized AuNPs. It is anticipated that the intersection of microbiology and nanomaterial synthesis could pave the way to several new economic and eco-friendly approaches, for new interdisciplinary applications.

Experimental details

Isolation of sample

The collected soil sediment samples were placed in sterile polyethylene bags, closed tightly and stored in a refrigerator at 4°C until use. For the isolation of actinomycetes, soil samples were first mixed, suspended in sterile distilled water (1 g in 100 ml) and homogenized by vortexing, and then finally treated for 5–10 min via sonication according to Ouhdouch methodology (Ouhdouch et al. 2001). The treated samples were serially diluted up to 10–6 and spread

(0.1 ml) over the surface of starch casein agar (SCA) medium (pH 7.2) supplemented with 25 μg ml—1cycloheximide to inhibit fungal growth, and 10 μg/ml nalidixic acid to inhibit the bacteria capable of swarming, without affecting the growth of actinomycetes. All of the inoculated plates were incubated for 7–10 days at 30°C.

Morphological and physiological characteristics

Cultural characteristics of strain *S. hygroscopicus* were assessed visually in 14-day-old cultures grown on various International Streptomyces Project (ISP) media (Shirling and Gottlieb 1966) and Bennett's agar medium. Micro morphology and sporulation were observed under light microscopy via an inclined coverslip technique (Williams et al. 1989) on starch casein agar after 7 days of incubation at 30°C. Colours of aerial and substrate mycelia were determined and recorded using National Bureau of Standards (NBS) Colour Name Charts. The spore chain morphology and spore surface ornamentation were assessed via scanning electron microscopy (JEOL) of 14-day-old cultures grown on agar medium (Fig not shown).

Culture and synthesis of AuNPs

The *S. hygroscopicus* strain BDUS 49 was isolated from deep sea sediment. Their partial 16S rRNA gene sequences were deposited in Genbank under accession no. GU195049. The active strain of *S. hygroscopicus* was employed in the present study. It was grown in sterile nutrient broth (Sigma) (pH6.5) and the flasks were incubated with shaking at 30°C and 200 rpm for 5 days, cells were harvested via centrifugation at 5,000 rpm for 30 min and washed three times with de-ionized water. The harvested cells were then resuspended in DI water and 1×10^{-3} M $HAuCl_4$ aqueous solution was added to different flasks. The reactants were adjusted to neutral pH using 0.1 M NaOH solution. The whole mixture was maintained in the laboratory under ambient conditions and the reactions were carried out for 48 h. During incubation periods, the color of the reaction solution gradually turned from pale yellow to pink red, thus indicating the formation of AuNPs. Prior to further measurements, the AuNPs solution was sonicated mildly for 30 s.

Absorbance and analytical measurement

The absorbance spectrum of the sample was obtained in a wavelength range of approximately 300–700 nm using the UV–Visible spectrophotometer (Optizen 3220, MECASYS) at regular intervals. The crystallinity and identity of the nanoparticles were investigated using an X-ray diffractometer (XRD, Scintag-SDS 2000) at 40 kV/20 mA using continuous scanning 2θ mode. The elemental composition of a molecule/species was notified through EDXA analysis by FE-SEM (HITACHI S-4700).

Morphological characterization of green synthesized Au nanoparticle

Morphological characterizations were conducted with transmission electron microscopy (Tecnai G^2 F30 TEM), field emission scanning electron microscopy (FE-SEM) (HITACHI S-4700) and bio-AFM (Atomic force Microscopy—Nanowizard II). For HRTEM, samples were prepared on carbon-coated copper grids and the films on the TEM grids were allowed to stand for 2 min, following which the extra solution was removed using a blotting paper and the grid was allowed to dry prior to measurement. For FE-SEM, samples were mounted on specimen stubs with double-sided adhesive carbon tape coated with platinum in a sputter coater and examined under field emission scanning electron microscopy. For bio-AFM, the samples were drop-coated on glass substrates and air-dried. Intermittent contact mode (air) was applied to obtain topographical images of the AuNPs.

Electrochemical study: cyclic voltammetry

CVs analysis was carried out using the three-electrode configuration of a Biologic Science Instrument SP-300. Platinum (Pt) and Ag/AgCl electrodes were used as counter and reference electrodes, respectively. Electrochemically-coated copper (I) oxide (Cu_2O) on Pt substrate (Cu_2O–Pt) were employed as the working electrodes and thoroughly surface-cleaned using anhydrous ethanol and acetone for 5 min. The procedure for electrochemical deposition of Cu_2O structures on Pt substrate was obtained from the reported literature (Sastry et al. 1998). Afterward, oxygen air plasma treatment was conducted for 500 s to render the surface hydrophilic, which will enhance the

1,2-ethanedithiol activation on the Cu2O–Pt electrode surface. The plasma-treated Cu2O–Pt electrode was subsequently soaked in a petri dish containing 1 mM 1,2-ethanedithiol for 12 h. Afterwards, the dithiol-activated Cu2O–Pt electrode is washed for 2 min with DI water. An appropriate amount (100 µl) of AuNPs–Methylene blue (AuNPs–MB) was drop-casted on the surface of the thiol-pretreated Cu2O–Pt electrode and permitted to form a monolayer for 12 h. CVs were recorded in 10 mM phosphate-buffered saline (PBS; pH 7.4) solutions using 1,3-diphenylbenzofuran (DPBF) as a probe molecule in the potential range of −0.2 to +0.450 V and at a scan rate of 20 mV/s. Each of the CV scans was repeated three times.

Minimum inhibitory concentration of AuNPs

The antibacterial activity of the AuNPS was tested using growth inhibition studies against Gram-positive and Gram-negative bacteria such as, *Bacillus subtilis* KACC 14394 (*B. subtilis*), *Staphylococcus aureus* KACC 13236 (*S. aureus)*, *Enterococcus faecalis* KACC 13807 (*E. faecalis)*, *Staphylococcus epidermidis* KACC 13234 (*S. epidermidis)*, *Escherichia coli* KACC 10005 (*E. coli)*, *Salmonella typhimurium* KACC 10763 *(S. typhimurium)*. All the strains were purchased from the Korean Agriculture Culture Collection Centre. Minimum inhibitory concentrations (MIC) of the synthesized AuNPS were determined via an MTT assay using a 96-well microtitre plate. The mean live cells of six pathogenic organisms were inoculated, where the final volume in each microwell plate was adjusted to 0.2 ml, and incubated overnight at 30°C. After incubation, the microwell plates were read at 590 nm using an ELISA reader (Emax precision microplate reader) prior to and after incubation to determine the MIC values.

Results and discussion

The genus *Streptomyces* is a well-known commercial organism for use in the production of biologically active compounds, antiparasitic agents, antibiotics, and cytochrome P450 enzymes. Herein, we have reported that the resuspended solution of *S. hygroscopicus* in DI water became a pale yellow solution upon the addition of $HAuCl_4$. This color change has been attributed to the reduction of aqueous chloroaurate ions to metallic gold (AuO) upon exposure to *S. hygroscopicus* cells. The color of the reaction solution turned purple to dark red, thereby indicating the formation of AuNPs. Previous studies (Mukherjee et al. 2001; Ahmad et al. 2002; Senapati et al. 2005) have shown that NADH- and NADH-dependent enzymes are important factors in the biosynthesis of metal nanoparticles. The accurate mechanism underlying the reduction of gold ions has yet to be elucidated for *S. hygroscopicus.* The reduction appears to be initiated via electron transfer from NADH-dependent enzymes as an electron carrier. This may play a key role in these biosynthetic and biotransformation reactions (Chun et al. 2006). The mechanism involved in this study involves the dual function of *S. hygroscopicus* active compounds as both a reducing and stabilizing agent.

UV–Vis absorption spectroscopy analysis of fabricated AuNPs

The bio-transformation process of the reaction solution is observed via visual inspection as well as measurements of UV–Vis absorption spectroscopy (Fig. 1). The UV–Vis spectrum illustrated in Fig. 1 (*Curve A*) shows no indication of an absorption peak in the region of 300–900 nm for the *S. hygroscopicus* supernatant. The UV–Vis spectra results showed that the reaction solution evidences an absorption maximum at approximately 540 nm attributable to the surface plasmon resonance band (SPR) of the

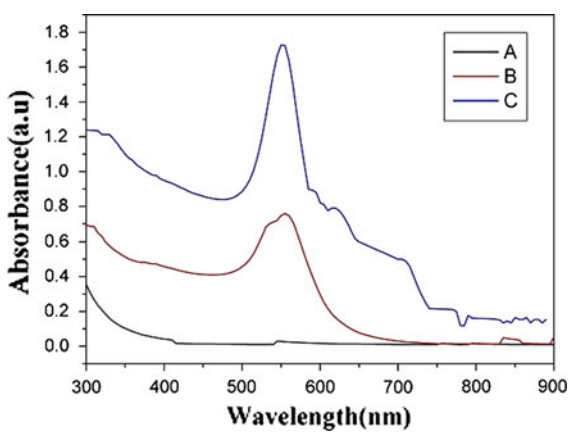

Fig. 1 UV–Vis absorption spectrum of Au nanoparticles after 48 h of reaction. **a** *S. hygroscopicus* supernatant. **b, c** UV–Vis absorption spectra of gold nanoparticles after the 24 and 48 h reaction in neutral pH. **c** pH at 4

spherical AuNPs after 48 h reaction (*Curve B*). When the pH was decreased, a number of mixed nanoplates observed as compared to the spherical AuNPs. Synthesized AuNPs were confirmed by sampling the reaction mixture at regular intervals and the absorption maxima were scanned by UV–vis spectra.

X-ray diffraction pattern of fabricated AuNPs

In order to confirm the crystal phase of the AuNPs, XRD analysis was carried out. Figure 2 shows the XRD patterns of the nanoparticles. The diffraction features appearing at $2\theta = 38.1$, 44.3, 64.5, 77.5 and 81.7 correspond to the (111), (200), (220), (311) and (222) planes of the standard face-centered cubic phase of Au, respectively. The lattice constant calculated from this pattern was 'a' = 4.086 Å and the data obtained matched with the database of the Joint Committee on Powder Diffraction Standards (JCPDS) file No. 04-0783. The average grain size of the AuNP formed in the bioreduction process was determined using Scherr's formula: $d = (0.9\lambda \times 180°)/\beta \cos \theta\pi$. The diffracted intensities were recorded from 20 to 90 degrees 2θ angles.

Morphological observations of fabricated nanoparticles

Figure 3 shows the various shapes and sizes of AuNPs formed with changes in pH. Thus, the morphology and

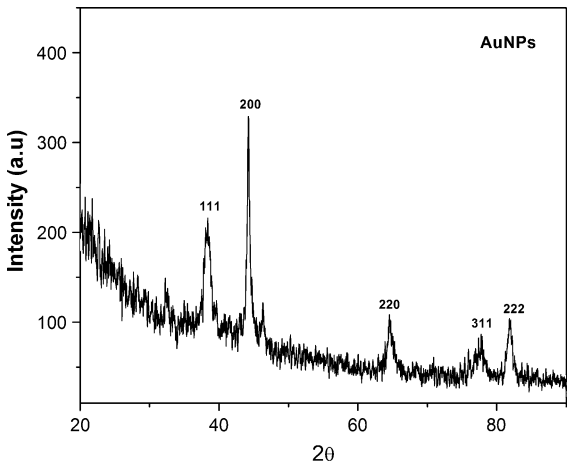

Fig. 2 XRD pattern recorded from fabricated AuNPs. In spectrum (recorded from powder form of synthesized AuNPS) the diffractions at 38.5°, 44°, 64.5°, 76.9° and 81.7° 2θ can be indexed to the (111), (200), (220) (311) and (222) planes of the face-centered cubic (fcc) gold, respectively

dimension of the AuNPs are noted to depend on the gold precursor solution, pH, and reaction time. All the above factors are found to be interdependent.

Figure 3 also shows the well-separated spherical AuNP in the range of 2–10 nm at neutral pH. When the pH was decreased, a number of hexagonal and pentagonal nanoplates were noted in the reaction solution at room temperature (Fig. 3c, d). The HR-TEM images supported the production of multidimensional nanostructures under different pH conditions—the range of nanoplates is 30 nm to 1.5 micron. A crystallite image (Fig. 3e, f, g) shows the atomic arrangement of spherical, pentagonal and hexagonal AuNPs. The multidimensional gold particles were synthesized as described above by varying the pH value of the solution mixtures while keeping the other conditions constrant. Figure 4 provides further insights into the size and shape morphology details of the nanoparticles. The FE-SEM micrographs also demonstrate the size and shape of the particles. The diameter of the spherical gold particle is approximately 10–20 nm (Fig. 4a). Figure 4b–d confirms the formation of multidimensional nanoplates in the size range of 30 nm–1.5 microns. Additional information on the formation and stabilization of AuNPs by green synthesis was examined by EDXA (Fig. 5) combined with FE-SEM. The EDXA spectrum revealed a strong signal for gold. Other peaks corresponding to Si, O and Pt were also observed, most likely because of the borosilicate glass and the fact that the sample was sputter-coated with platinum for FE-SEM. Furthermore, the Bio-AFM image was consistent with the HRTEM and FE-SEM images (Fig. 6).

Cyclic voltammetry analysis of AuNPs

Electrodes with significant chemical modifications are used extensively as a sensitive and selective analytical method for the detection of biologically important compounds. Generally, chemical modifications of electrodes are incorporated using a broad variety of materials such as inorganic and organic compounds (Veerapandian et al. 2011), conducting polymers, metal of different forms, reviewed elsewhere (Ragupathy et al. 2010). The electrochemical properties of AuNPs for a broad range of chemical and biochemical analyses have been thoroughly evaluated (Shaojun and Erkang 2007). In an effort to evaluate the electrochemical properties of current biologically synthesized

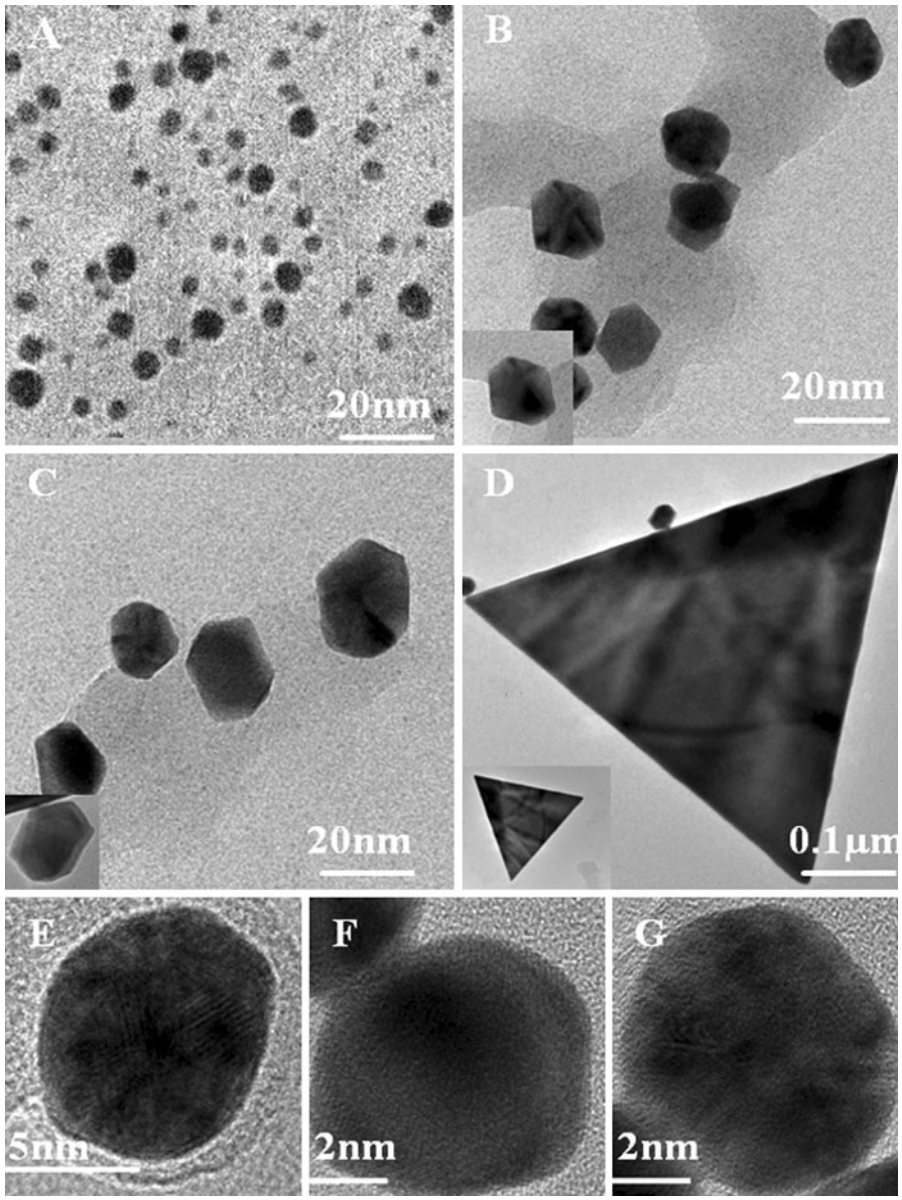

Fig. 3 HR-TEM images of multishaped AuNPs after 48 h of reaction **a** Neutral pH, **b**–**d** pH 4, **e**–**g** crystallite structure of AuNPs

AuNPs, a well-known electroactive cationic dye MB (redox indicator) is coated on the surface of AuNPs via an ultrasonication process. The physically adsorbed AuNPs–MB were then drop-casted on alkane dithiol-pretreated Cu2O–Pt substrate and used as working electrode. The resulting CVs were measured under PBS and PBS–DPBF. We previously demonstrated the electrochemical properties of MB-coated Ag–SiO_2NPs in the presence of DPBF as an analyte probe in which the MB–Ag–SiO_2NPs were coated onto the surface of an Au–PCB electrode. The surface modification of different NPs on electrode surface may be attributable to the measurement of the presence of a constant analyte in electrolyte solution via significant changes in the CVs. As the materials fabricated in the current approach are AuNPs, we have selected a different electrode composed of Cu2O–Pt as the substrate for observation of the specific response from AuNPs–MB. Here, it is worth noting that the utilization of Cu2O–Pt substrate as a working electrode is

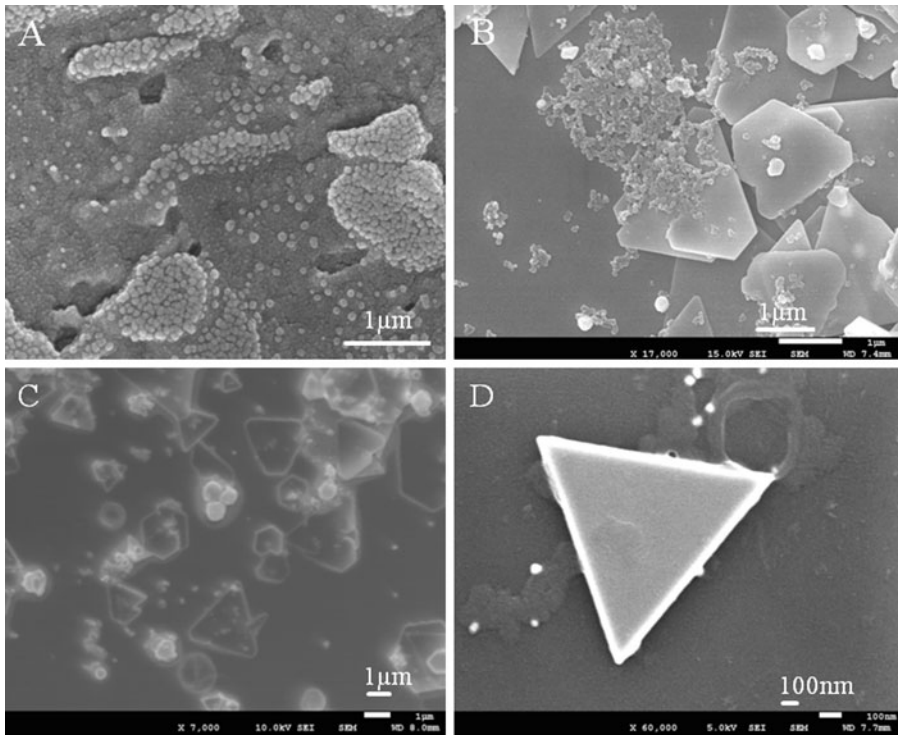

Fig. 4 FE-SEM images of multishaped AuNPs after 48 h of reaction **a** Neutral pH, **b–d** pH 4

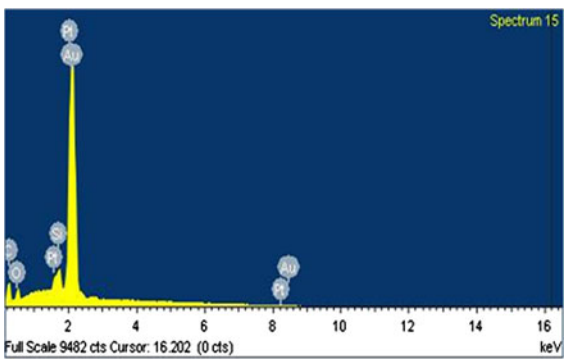

Fig. 5 EDXA spectra of cell-free extract following the reduction of $AuCl_4^-$ ions recorded from FE-SEM–EDX

attributable to its convenient availability, rather than because of any other specialization. Figure 6 shows the typical CVs for AuNPs–MB-modified Cu2O–Pt electrodes under different volume ratio of DPBF in PBS buffer. As observed in Fig. 7a—black trace), the control sample shows a short intense cathodic peak potential (E_{pc}) centered at 0.112 V and a broad weak anodic peak potential (E_{pa}) at −0.041 V. Figure 7b–e shows the electrochemical signal in presence of probe DPBF (100, 200, 300 and 400 μl); CVs show notable variations in cathodic peaks with a reduced current signal of approximately 0.107, 0.106, 0.093 and 0.092 mA, respectively. This may be due to the irreversible reaction between DPBF and electronically excited singlet delta oxygen ($^1\Delta_g$). It has been demonstrated that the cationic dye MB is auto-oxidizable and can donate electrons, thereby readily reducing the levels of other compounds. This reaction mechanism of interaction was recently reported from MB-coated phosphonate-terminated SiO_2NPs (PSiNPs) by detecting the maximum absorbance using UV–visible spectroscopy (Xiaoxiao et al. 2009). That report demonstrates that DPBF reacts with $^1O_2$, which induces a reduction in the intensity of the DPBF absorption band at 400 nm and thereby detects the generation of singlet oxygen from MB–PSiNPs. Likewise, in this study, the AuNPs modified with MB electro-actively generated the singlet oxygen species which mediates the irreversible reaction with DPBF and also induces significant changes in the CVs. Owing to the addition and increasing concentration of the analyte from 100 to 400 μl in the desired electrolyte solution, a shift in the cathodic peak potential, disappearance of the anodic peak and reduced current

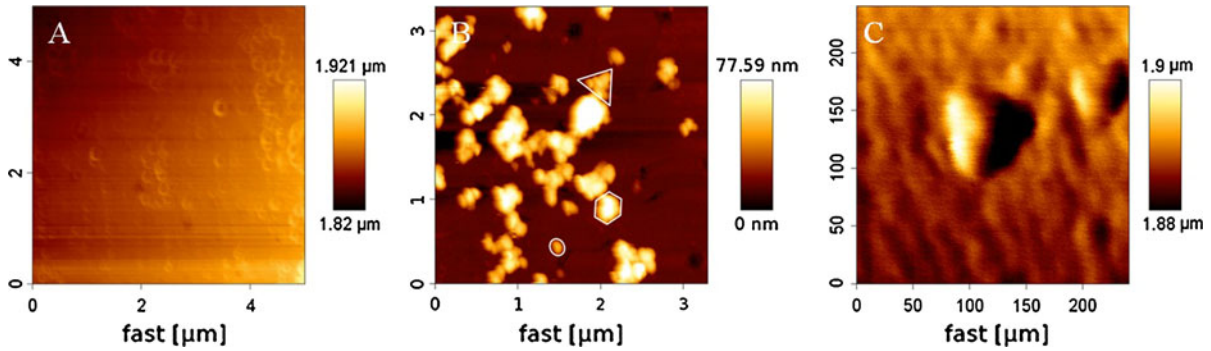

Fig. 6 Bio-AFM image of multishaped AuNPs after 48 h reaction. **a** Neutral pH. **b, c** pH 4

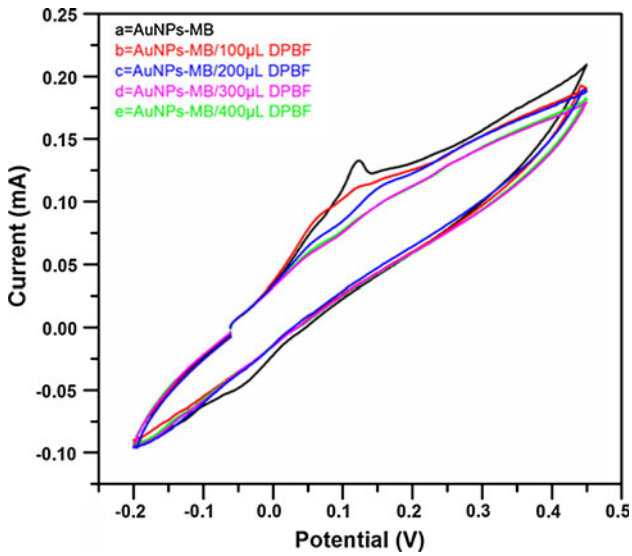

Fig. 7 Cyclic voltammetry analysis of AuNPs. **a** AuNps with MB. **b–e** Au–MB with 100, 200, 300, and 400 µl of DPBF, respectively

intensity have been observed as compared to AuNPs–MB (without DPBF) alone. Figure 8 depicts the monolayer of AuNPs–MB coated on the Cu2O–Pt substrate after electrochemical scanning. The image clearly depicting the synthesized multidimensional nanoparticles could function as electroactive nanostructures and were successful in inducing the electrochemical reaction. This preliminary electrochemical response observed via the protocol devised in the current study allowed us to extend the application of the fabricated AuNPs for the construction of a broad range of electrochemical sensors.

Microtiter broth dilution method

The 96 well microtiter plate method was used to assess the MIC profile against six different pathogens. Kanamycin was used as a standard and AuNPs were used for antimicrobial screening. Table 1 shows the bacterial organisms and their MIC values. Among the six organisms selected for this study, maximal growth inhibition was observed when using *E. coli*, *S. typhimurium* and *S. aureus*. The minimal inhibition of these strains ranged from 64 to 128 µg/ml, which was almost equal to the MICs obtained using standard antibiotics. Furthermore, the MICs of AuNPs against *B. subtilis* KACC 14394, *S. epidermidis* KACC 13234 and *E. faecalis* KACC 13807 were measured to be 64,128 and 256 µg/ml. The AuNPs interacted with bacteria in all directions due to the multidimensional exposure of the NPs, which provided better interaction with microorganisms and enhanced antimicrobial activity. From the results of the antibacterial study, the MIC values are defined as the lowest concentration

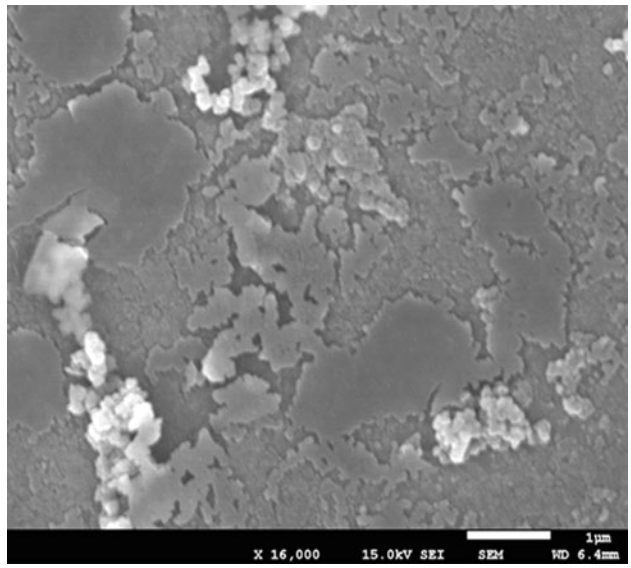

Fig. 8 FE–SEM image of AuNPs–MB-modified Cu_2O–Pt substrate after CVs scan

Table1 Minimum inhibitory concentration (MIC) of AuNPs against pathogenic bacterial strains

Bacterial strains	AUNPs MIC (μg/ml)	Kanamycin MIC (μg/ml)
Bacillus subtilis KACC 14394	64	8
Staphylococcusaureus KACC 13236	32	8
Enterococcus faecalis KACC 13807	256	16
Staphylococcus epidermidis KACC 13234	128	8
Escherichia coli KACC 10005	32	8
Salmonella typhimurium KACC 10763	32	8

Control undiluted AuNPs

of the compound that inhibited 80% of bacterial growth.

Conclusion

From our experiments we have demonstrated that, the multidimensional AuNPs (e.g., triangle and hexagon) were synthesized using the culture supernatant of *S. hygrocopicus.* Structural elucidations of the fabricated nanoparticle were well ensured by UV–vis and EDXA studies. The X-ray diffraction study further confirmed the identity and crystallinity of fabricated nanoparticles. Moreover, we have demonstrated the electrochemical and antimicrobial activity of nanoparticle synthesized by CVs and MIC analysis. This method has effectively provided a simple, green, biochemical route for the production of multishaped AuNPs, although the solution is highly stable. The methods described herein appear to be a better choice for achieving nanomaterials of controlled shapes and sizes than the chemical methods currently available. A purely green-chemistry-based biological method appears promising for extension to other structures.

Acknowledgment This work was supported by Kyungwon University research fund in 2011(2011-R295).

References

Ahmad A, Mukherjee P, Mandal D, Senapati S, Khan MI, Kumar R, Sastry M (2002) Enzyme mediated extracellular synthesis of CdS nanoparticles by the fungus, *Fusarium oxysporum*. J Am Chem Soc 124:12108–12109

Ahmad A, Senapati S, Khan MI, Kumar R, Sastry M (2003) Extracellular biosynthesis of monodisperse gold nanoparticles by a novel extremophilic actinomycete, *Thermomonospora* sp. Langmuir 19:3550–3553

Bethell D, Schriffrin DJ (1996) Nanotechnology and nucleotides. Nature 382:581

Brown S, Sarikaya M, Johnson E (2000) A genetic analysis of crystal growth. J Mol Biol 299:725–735

Brus LJ (1994) Luminescence of silicon materials: chains, sheets, nanocrystals, nanowires, microcrystals, and porous silicon. Phys Chem 98:3575–3581

Chun YJ, Shimada T, Waterman MR, Guengerich FP (2006) Understanding electron transport systems of *Streptomyces* cytochrome P450. Biochem Soc Trans 34:1183–1185

Dameron CT, Reese RN, Mehra RK, Kortan AR, Carroll PJ, Steigerwald ML, Brus LE, Winge DR (1989) Biosynthesis of cadmium sulphide quantum semiconductor crystallites. Nature 338:596–597

Duan XF, Huang Y, Agarwal R, Lieber CM (2003) Single nanowire electrically driven lasers. Nature 421:241–245

Grubbs RB (2007) Solvent-tuned structures. Nat Mater 6:553–555

Heath JR, Kuekes PJ, Snider GS, Williams SR (1998) A defect-tolerant computer architecture: opportunities for nanotechnology. Science 280:1716–1721

Herman A, Addadi L, Weiner S (1988) Interactions of sea-urchin skeleton macromolecules with growing calcite crystals a study of intracrystalline proteins. Nature 331:546–548

Hosea M, Greene B, McPherson R, Henzl M, Alexander MD, Darnall DW (1986) Accumulation of elemental gold on the alga *Chlorella vulgaris*. Inorg Chim Acta 123:161–165

Iosin M, Toderas F, Baldeck P, Astilean SJ (2008) In vitro biosynthesis of gold anotriangles for Surface-Enhanced Raman spectroscopy. Optoelectron Adv Mater 10:2285–2288

Johnson JC, Yan HQ, Schaller RD, Haber LH, Saykally RJ, Yang PD (2001) Single nanowire lasers. J Phys Chem B 105:11387–11390

Katz E, Willner I, Wang J (2004) Electroanalytical and bioelectroanalytical systems based on metal and semiconductive nanoparticles. Electroanalysis 16:19–44

Klaus T, Joerger R, Olsson E, Granqvist CG (1999) Silver-based crystalline nanoparticles, microbially fabricated. Proc Natl Acad Sci USA 96:13611–13614

Komeili A, Vali H, Beveridge TJ, Newman DK (2004) Magnetosome vesicles are present before magnetite formation, and MamA is required for their activation. Proc Natl Acad Sci USA 101:3839–3844

Kroger N, Deutzmann R, Sumper M (1999) Polycationic peptides from diatom biosilica that direct silica nanosphere formation. Science 286:1129–1132

Labrenz M, Druschel GK, Ebert TT, Gilbert B, Welch SA, Kemner KM, Logan GA, Summons RE, Stasio GD, Bond PL, Lai B, Kelly SD, Banfield JF (2000) Sphalerite (ZnS) deposits forming in natural biofilms of sulfate reducing bacteria. Science 290:1744–1747

Lang C, Schuler D, Faivre D (2007) Synthesis of magnetite nanoparticles for bio- and nanotechnology: genetic engineering and biomimetics of bacterial magnetosomes. Macromol Biosci 7:144–151

Lee J, Hwang S, Lee H, Kwak J (2004) Bimetallic clusters by underpotential deposition on layered Au nanoparticle films. J Phys Chem B 108:5372–5379

Lovley DR, Stolz JF, Nord GL Jr, Phillips EJP (1987) Anaerobic production of magnetite by a dissimilatory iron-reducing microorganism. Nature 330:252–254

Mukherjee P, Ahmad A, Mandal D, Senapati S, Sainkar SR, Khan MI, Ramani R, Parischa R, Ajayakumar PV, Alam M, Sastry M, Kumar R (2001) Bioreduction of $AuCl_4^-$ ions by the fungus, *Verticillium* sp. and surface trapping of the gold nanoparticles formed. Angew Chem Intl Edn Eng 40:3585–3588

Ouhdouch Y, Barakate M, Finance C (2001) Actinomycetes of Moroccan habitats: isolation and screening for antifungal activities. Eur J Soil Biol 37:69–74

Ragupathy D, Gopalan AI, Lee K-P (2010) Electrocatalytic oxidation and determination of ascorbic acid in the presence of dopamine at multiwalled carbon nanotube-silica network-gold nanoparticles based nanohybrid modified electrode. Sensor Actuat B: Chem 143:696–703

Sadhasivam S, Shanmugam P, Yun KS (2010) Biosynthesis of silver nanoparticles by *Streptomyces hygroscopicus* and antimicrobial activity against medically important pathogenic microorganisms. Colloid Surf B: Biointerfaces 81:358–362

Sastry M, Patil V, Sainkar SRJ (1998) Electrostatically controlled diffusion of carboxylic acid derivatized silver colloidal particles in thermally evaporated fatty amine films. Phys Chem B 102:1404–1410

Schmid G (1998) Lifeng CF metal clusters and colloids. Adv Mater 10:515–526

Senapati S, Ahmad A, Khan MI, Sastry M, Kumar R (2005) Extracellular biosynthesis of bimetallic Au–Ag alloy nanoparticles. Small 1:517–520

Shaojun G, Erkang W (2007) Synthesis and electrochemical applications of gold nanoparticles. Anal Chim Acta 598:181–192

Shirling EB, Gottlieb D (1966) Methods for characterization of *Streptomyces* species. Int J Syst Bacteriol 16:313–340

Tang ZY, Kotov NA, Giersig M (2002) Spontaneous organization of single CdTe nanoparticles into luminescent nanowires. Science 297:237–240

Veerapandian M, Subbiah R, Lim G-S, Park S-H, Yun KS, Lee M-H (2011) Copper–glucosamine microcubes: synthesis, characterization and C-reactive protein detection. Langmuir 27:8934–8942

Williams ST, Sharp ME, Holt JG (1989) Bergey's manual of systematic bacteriology, vol 4. Williams and Wilkins, Baltimore, pp 2492–2504

Wong SS, Joselevich E, Woolley AT, Cheung CL, Lieber CM (1998) Covalently functionalized nanotubes as nanometer probes for chemistry and biology. Nature 394:52–55

Xiaoxiao H, Xu W, Kemin W, Bihua S, Luo H (2009) Methylene blue-encapsulated phosphonate-terminated silica nanoparticles for simultaneous in vivo imaging and photodynamic therapy. Biomaterials 30:5601–5609